

RESEARCH ARTICLE

10.1002/2014JF003417

Key Points:

- Coseismic slope stability models rarely consider slope-normal accelerations
- Laboratory tests subjected sediment to variably-phased normal and shear stress
- Wave phasing controls the magnitude of coseismic landslide displacement

Correspondence to:

M. J. Brain,
matthew.brain@durham.ac.uk

Citation:

Brain, M. J., N. J. Rosser, J. Sutton, K. Snelling, N. Tunstall, and D. N. Petley (2015), The effects of normal and shear stress wave phasing on coseismic landslide displacement, *J. Geophys. Res. Earth Surf.*, 120, 1009–1022, doi:10.1002/2014JF003417.

Received 14 DEC 2014

Accepted 7 MAY 2015

Accepted article online 12 MAY 2015

Published online 6 JUN 2015

The effects of normal and shear stress wave phasing on coseismic landslide displacement

Matthew J. Brain¹, Nick J. Rosser¹, Jerry Sutton², Karl Snelling², Neil Tunstall¹, and David N. Petley³

¹Department of Geography and Institute of Hazard Risk and Resilience, Durham University, Durham, UK, ²GDS Instruments, Hook, UK, ³School of Environmental Science, University of East Anglia, Norwich, UK

Abstract Predictive models used to assess the magnitude of coseismic landslide strain accumulation in response to earthquake ground shaking typically consider slope-parallel ground accelerations only and ignore both the influence of coseismic slope-normal ground accelerations and the phase relationship between dynamic slope-normal and slope-parallel accelerations. We present results of a laboratory study designed to assess the significance of the phase offset between slope-normal and slope-parallel cyclic stresses on the generation of coseismic landslide displacements. Using a dynamic back-pressured shearbox that is capable of simulating variably phased slope-normal and slope-parallel dynamic loads, we subjected sediment samples to a range of dynamic loading scenarios indicative of earthquake-induced ground shaking. We detail the variations in strain accumulation observed when slope-normal and slope-parallel stresses occur independently and simultaneously, both in and out of phase, using a range of dynamic stress amplitudes. Our results show that the instantaneous phasing of dynamic stresses is critical in determining the amount of coseismic landslide displacement, which may vary by up to an order of magnitude based solely on wave-phasing effects. Instantaneous strain rate is an exponential function of the distance normal to the Mohr Coulomb failure envelope in plots of shear stress against normal effective stress. This distance is strongly controlled by the phase offset between dynamic normal and shear stresses. Our results demonstrate that conditions considered by conventional coseismic slope stability models can either overestimate or underestimate earthquake-induced landslide displacement by up to an order of magnitude. This has important implications for accurate assessment of coseismic landslide hazard.

1. Introduction

Earthquake-triggered landslides represent a significant hazard [Keefer, 1984; Marano *et al.*, 2010; Petley, 2012] and play a major role in orogen-scale sediment mobilization [Hovius *et al.*, 2011; Li *et al.*, 2014; Parker *et al.*, 2011]. Understanding the controls on, and estimating the magnitude of, coseismic landslide displacement during seismic loading is critical for quantifying hazard and risk [Guzzetti *et al.*, 1999; Jibson *et al.*, 2000] and determining the impacts associated with earthquakes [Keefer, 1994; Malamud *et al.*, 2004]. Directly estimating coseismic landslide displacement, rather than relying on correlations with empirical seismic data sets [Keefer, 1984], has the potential to improve understanding of the spatial and temporal patterns of earthquake-triggered landslides [Jibson, 2007]. However, the accuracy of direct estimation techniques remains limited due to the combined difficulty of capturing the complexity of coseismic dynamic stresses within hillslopes [Bray and Travararou, 2007; Rathje and Antonakos, 2011; Rathje and Saygili, 2009; Saygili and Rathje, 2008; Wasowski *et al.*, 2011] and undertaking realistic simulations thereof in the laboratory [Liao *et al.*, 2011; Sassa *et al.*, 2004].

Coseismic landslide displacement is most commonly estimated at the regional scale [e.g., Dreyfus *et al.*, 2013; Jibson *et al.*, 2000] by combining a dynamic slope stability model with measurements or approximations of the magnitude of ground shaking [Jibson, 2011] using the Newmark [1965] sliding block model. When used to assess slope stability, and when used in its most simple form (see Jibson [2011] for further detail and rationale), this model considers a rigid friction block on a planar hillslope subjected to earthquake accelerations. The so-called Newmark displacement, D_N , is generated when downslope acceleration overcomes basal frictional resistance, reducing the slope factor of safety (FS, the ratio of shear resistance to shear stress) below unity, causing the block to become unstable. The necessary critical acceleration, a_c , is calculated using static (aseismic) stress conditions [Newmark, 1965] as

$$a_c = (FS - 1)g \sin \alpha \quad (1)$$

where α is the shear (sliding) surface angle and g is gravitational acceleration (9.81 m/s^2). Using strong-motion ground displacement records or some approximation thereof [Ambraseys and Menu, 1988; Jibson, 2007], cumulative landslide displacement is subsequently estimated through two successive integrations with respect to time of the parts of the slope-parallel acceleration time history that are greater than a_c . First, acceleration is integrated to calculate velocity of the sliding block for the period of time when acceleration exceeds a_c . The second integration to obtain displacement is undertaken over a different timeframe because the block is still moving, though decelerating, when the acceleration drops to a value lower than a_c [Jibson, 1993]. Romeo [2000] provided a summary of the assumptions and limitations of the Newmark [1965] approach. Of these, Romeo [2000] highlights two key assumptions: first, that static and dynamic strengths are considered to be the same and second, that increases in pore water pressure during seismic shaking do not occur, and hence do not affect shearing response via their control on normal effective stresses and frictional strength. These assumptions are not met in all situations [Newmark, 1965; Trandafir and Sassa, 2005; Danneels et al., 2008; Wang and Sassa, 2009; Wasowski et al., 2011; Schulz and Wang, 2014]. However, where the assumptions of the Newmark [1965] method, and in particular conditions of constant strength and no excess pore water pressures, are met, the Newmark [1965] method can be a potentially powerful tool for use in local to regional seismic risk assessment [Jibson et al., 2000] and has been widely applied, from the laboratory [Wartman et al., 2005] to both hillslope and regional scales [Jibson et al., 2000; Wilson and Keefer, 1983].

The input acceleration time history used to undertake Newmark [1965] analysis is key, exerting a first-order control on the magnitude of estimated permanent displacement. Typically, the slope-parallel acceleration component is used in Newmark [1965] analysis. Alternatively, in more simplified analyses (see Jibson [2011] for a more detailed summary), the horizontal acceleration component is used on the implicit assumption that the majority of the resultant dynamic accelerations (and hence stresses) are applied in slope-parallel directions in slopes $< 45^\circ$.

The infinite slope model typically used to calculate the FS, and the use of the Coulomb equation therein [Taylor, 1948], indicate that coseismic slope-normal accelerations can alter the balance of forces acting within a hillslope independently of changes resulting from slope-parallel accelerations [Ingles et al., 2006]. Seismographic records from earthquake events clearly exhibit conditions in which the instantaneous ratio of vertical to horizontal acceleration exceeds unity [Aoi et al., 2008; Bradley and Cubrinovski, 2011]. A positive (i.e., into the slope) slope-normal coseismic ground acceleration reduces resistance to shear by temporarily reducing interparticle friction [see also Aoi et al., 2008], thereby decreasing instantaneous a_c . As a result, the magnitude of D_N in response to downslope cyclic slope-parallel (shear) stresses under conditions where slope-normal (positive into the slope) and slope-parallel (positive downslope) accelerations are in phase would be increased. In contrast, an instantaneous out-of-slope acceleration would momentarily increase resistance to shear, increase a_c , and permit reduced strain accumulation as out-of-phase downslope coseismic shear stresses are applied. An additional key assumption of conventional Newmark [1965] and associated analyses is that slope-normal accelerations have a negligible control on D_N and, hence, that the instantaneous phase relationship between coseismic cyclic slope-normal and slope-parallel ground accelerations does not have a significant effect on the magnitude of coseismic strain accumulation. In turn, this rests on the assumption that instantaneous phase relationships between normal and shear stresses during an earthquake event are random, such that a_c is as likely to increase as it is to decrease [Matasovic et al., 1998]. Hence, while transient displacements may be greater or less than those predicted using conventional Newmark [1965] analysis that ignores slope-normal stresses, these effects have been assumed to average out [Jibson, 2011] creating no net difference in D_N from that predicted when considering slope-parallel stresses only. For this averaging to be valid, D_N resulting from a single cycle of in-phase normal and shear stresses must be reduced in magnitude relative to standard (shear-only) Newmark [1965] analysis by the same amount that out-of-phase normal and shear stresses would cause D_N to increase relative to standard (shear-only) Newmark [1965] analysis. This implicitly assumes that strain rates vary linearly relative to the baseline (aseismic) stress state, regardless of the instantaneous normal and shear stress phase relationship and, hence, the dynamic/seismic stress state at the landslide shear surface.

The potential inaccuracies of the standard Newmark [1965] approach have previously been observed in field and modeling studies. Huang et al. [2001], for example, compared estimations of D_N using standard Newmark

[1965] analysis with those that also considered slope-normal accelerations, using ground motion records from the 1999 Chi Chi earthquake, Taiwan. They noted that inclusion of slope-normal accelerations approximately doubled calculated D_N and, hence, significantly affected estimations of coseismic slope deformation. More generally, *Ingles et al.* [2006] used a modeling approach to examine the role of vertical ground accelerations and, hence, slope-normal accelerations in controlling coseismic landslide displacements. They concluded that inclusion of vertical accelerations in *Newmark* [1965] analysis can considerably affect calculations of coseismic slope stability. However, neither study directly considered dynamic normal effective and shear stress wave-phasing effects from a mechanical/process perspective and how this may affect strain accumulation. Indeed, while widely and implicitly accepted, the assumption that normal and shear stress wave-phasing effects are not important in determining the magnitude of D_N has not been rigorously tested until now.

Using a laboratory instrument built specifically to simulate coseismic landslide deformation and failure in direct shear conditions analogous to those assumed in the *Newmark* [1965] sliding block model, we have undertaken the first empirical assessment of the significance of the phase offset between slope-normal and slope-parallel cyclic stresses on the generation of coseismic landslide displacements. If significant differences in coseismic shear strain accumulation result from wave-phasing effects at the laboratory scale, the implications for coseismic landslide hazard assessment may be considerable because wave-phasing effects are not currently considered in existing coseismic slope stability models.

2. Materials and Methods

2.1. Sediment Material

Since we were interested in potentially subtle differences in stress-strain relationships under varying dynamic loading conditions and normal and shear stress phase relationships, we required a sediment that displayed highly uniform stress-strain behavior akin to that observed in normally consolidated hillslope materials. We did not consider undisturbed natural sediments to be appropriate for our geotechnical testing program due to the inherent variability in shearing behavior they can display that results from variable sedimentary structure, stress history, and sampling effects [*Burland*, 1990]. Instead, we used a commercially available modeling sediment composed of polymer-coated particles of very coarse silt and very fine sand [*Blott and Pye*, 2001; *Friedman and Sanders*, 1978; *British Standards Institution*, 1999]. The polymer coating added a cohesive strength to the samples that aided uniform sample preparation and, hence, geotechnical behavior, but demonstrated lower sensitivity to moisture content than inclusion and use of clay minerals.

2.2. Geotechnical Testing Apparatus

We used a bespoke testing apparatus, named the Dynamic Back-Pressured Shearbox (DynBPS), to undertake our testing program. The DynBPS subjects samples (plan dimensions: 100 × 100 mm and depth: 20 mm) to direct shear along a defined shear surface (Figure 1). We consider direct shear to be the most representative of the conditions occurring during incipient translational and planar landslide failure. In a conventional shearbox (see *Head and Epps* [2011] and *Selby* [2005] for more detailed descriptions of the apparatus), sediment samples are placed within a cuboid shearbox vessel composed of upper and lower sections. During sample preparation, the upper and lower sections of the box are attached using clamping screws. The vessel is then mounted within a container which is subsequently flooded to encourage saturation. The chamber is exposed to atmospheric pressure; fluid pressure cannot be controlled or measured and so the true effective stress state of the sediment is not known. Through a normal loading ram, the sediment is loaded vertically to provide a normal total stress, simulating the weight of overlying material within a hillslope. Subsequently, the upper section of the box is lifted off the lower section to create a “shear gap” along which shearing can occur; the shear gap is approximately at the midheight of the sample. While keeping normal stress constant, the upper section of the box is then held in place as the lower section of the shearbox is displaced laterally. This is typically done by specifying a constant rate of strain and by measuring the resultant shear load required to effect shear strain. By dividing shear load by the cross-sectional area of the sample, shear stress can be calculated.

The DynBPS is an advanced direct shear apparatus (see *Barla et al.* [2010] and *Gan et al.* [1988] for further information about similar, yet nondynamic, direct shear machines) modified to permit control and

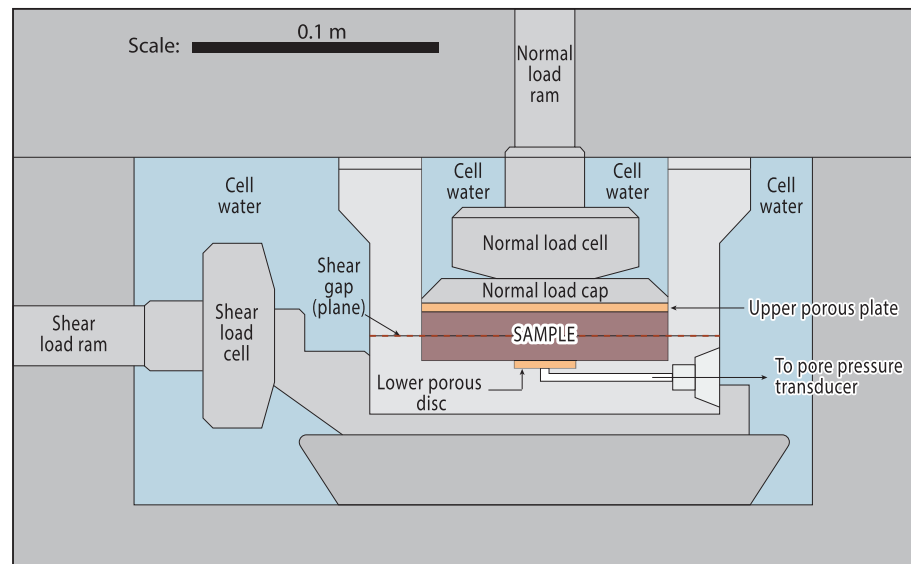


Figure 1. The internal components of the Dynamic Back-Pressured Shearbox (DynBPS) testing cell. See text for further details.

measurement of pore water pressure and application of dynamic normal and shear stresses. The shearbox is placed within a flooded, pressurized chamber. Fluid pressure (≤ 1 MPa; 1.0 kPa precision) within the chamber (and, hence, sample) is controlled by a hydraulic back pressure controller. Pore water pressure is measured at the base of the sample via a porous disc that is connected to a pressure transducer (0.1 kPa precision), which permits calculation of the normal effective stress acting on the sediment, expressed as

$$\sigma'_n = \sigma_n - u \tag{2}$$

where σ'_n is the normal effective stress (i.e., the stress carried by the sediment grains), σ_n is the total normal stress applied by the normal load ram, and u is pore water pressure.

Both axial (slope and shear surface normal) and horizontal (slope and shear surface parallel) loads are applied using electromechanical actuators and measured using load cells (axial/normal load ≤ 25 kN, 0.025 kN (0.1% full range) precision; horizontal/shear load ≤ 10 kN, 0.01 kN (0.1% full range) precision). Both normal and shear loads can be controlled under monotonic or dynamic (≤ 5 Hz) conditions using either load or displacement control. Critically, normal and shear forces can be controlled independently under dynamic conditions, permitting control of instantaneous wave phasing. Axial/normal displacement is measured using the internal motor encoder. The horizontal/shear displacement is measured internally using a 75 mm range rectilinear potentiometer with a linearity of 0.15% and hysteresis of 0.01 mm. The maximum shear displacement that can be achieved is 20 mm (i.e., 20% shear strain). When describing laboratory test results, we report values of strain (i.e., the ratio of total deformation to the initial dimensions of the sample, expressed as %) rather than those of displacement; use of strain permits more straightforward comparison between laboratory tests and field settings where dimensions differ. In short, the DynBPS permits replication of dynamic stresses in hillslopes during earthquakes. The accuracy and precision of the instrument, and the potential to independently vary dynamic normal and shear stresses, allow the effects of wave phasing to be assessed.

2.3. Geotechnical Testing

2.3.1. Saturation and Consolidation

To aid sample saturation, we flushed the sample and chamber with carbon dioxide for 1 h to displace pore air, since carbon dioxide is more soluble in water than air. We subsequently flooded the chamber with de-aired water and increased the chamber fluid (back) pressure and total normal stress such that the required level of normal effective stress, and associated consolidation, were achieved. During consolidation (and throughout shear testing) we monitored normal displacement. The shearbox laterally confines the sediment samples and prevents lateral strains from occurring, replicating the conditions experienced in real-world conditions [Powrie, 2004].

2.3.2. Monotonic Direct Shear Tests

We undertook three conventional baseline tests to determine the monotonic direct shear behavior of our sediment at normal effective stress values of 100, 200, and 300 kPa. The shearing stages of these (consolidated, drained) tests were displacement-controlled at a rate of 0.1 mm/min, equivalent to a shear strain rate of $0.1\% \text{ min}^{-1}$. This strain rate was sufficiently low to prevent generation of excess (i.e., above back pressure) pore water pressures; thus, we maintained a constant normal effective stress for the duration of each test. The purpose of these tests was to determine basic Mohr-Coulomb properties of the sediment and to assess volumetric change during shearing. These results were required to define the baseline stress conditions of the dynamic testing program.

2.3.3. Dynamic Direct Shear Tests

We focused on dynamic shear behavior at a baseline normal effective stress of 200 kPa in a set of 20 dynamic experiments. Following consolidation, we sheared the sample under displacement control (equivalent shear strain rate of $0.1\% \text{ min}^{-1}$) to a specified shear stress value defined on the basis of the drained monotonic direct shear results; application of an initial shear stress is required to mimic stresses in a real-world hillslope during aseismic conditions.

Following consolidation and initial shear, each subsequent dynamic phase was undertaken at 2 Hz and by simulating a sinusoidal waveform. We selected 2 Hz as our test frequency because it is sufficiently high to consider the effects of dynamic loading and wave phasing but low enough to prevent liquefaction. While we acknowledge the true complexity of real-world seismographic records [Wasowski *et al.*, 2011], we adopted a simplified seismic waveform (single frequency, sinusoidal) in our experimental study that is concerned with addressing fundamental controls on shearing behavior under dynamic conditions. The use of idealized, uniform waveforms is well-established in geotechnical testing [Christakos, 2003; Hyde *et al.*, 2006; Sağlam and Bakır, 2014]. In contrast, real-world seismographic records vary considerably in terms of their frequency and amplitude content, which can drive variations in drained and undrained shear behavior and strain accumulation during dynamic loading. If these effects were included in our dynamic tests, it would become impossible to isolate the effects of variable wave-phasing relationships on coseismic strain accumulation. While many recent studies examine the effects of real-world seismographic records on coseismic landslide behavior [Schulz and Wang, 2014; Wang and Sassa, 2009; Yuan *et al.*, 2014], the aim and approach of these studies is fundamentally different.

All dynamic tests were undertaken under load control by specifying baseline normal and shear loads, and dynamic load amplitudes, which permitted ongoing shear strain accumulation as occurs in real-world landslides during earthquakes. Displacement control under dynamic conditions would not simulate or permit this behavior. We simulated five wave-phasing scenarios which, in turn, represent a range of variably phased vertical and horizontal accelerations resolved relative to a landslide shear surface. We first considered dynamic shear stresses only (a scenario here termed "SO"), in which effective normal stress remains constant, simulating the conditions assumed in conventional *Newmark* [1965] analysis and providing a benchmark data set against which all other scenarios can be compared. Second, we considered dynamic normal stresses only ("NO"), holding shear stress constant. Third, we varied normal and shear stresses synchronously in phase ("IP"). Fourth, we assessed the effects of a 90° phase shift in normal relative to shear stresses ("OOP $_{90^\circ}$ "). Finally, we tested the effects of the normal and shear stresses being 180° out of phase ("OOP $_{180^\circ}$ "). For each scenario, we undertook four tests, each with a specified cyclic load amplitude to simulate different magnitudes of earthquake-induced ground shaking. Specified shear load amplitudes employed were approximately 15, 50, 100, and 150% of the baseline shear stress, respectively; the absolute resultant dynamic stress amplitude values are defined below on the basis of the results of the monotonic direct shear test results. During dynamic tests, data were recorded using a sampling frequency of 200 Hz.

3. Results

3.1. Monotonic Direct Shear Behavior

Stress-strain curves for monotonic, displacement-controlled direct shear tests at normal effective stresses (σ'_n) of 100, 200, and 300 kPa display plastic behavior, with a gradual, minor, and variable (≤ 5 kPa) reduction to a constant (residual) strength where shear strain $\varepsilon \geq 14\%$ (Figure 2). The stress-strain curves are typical of those observed for

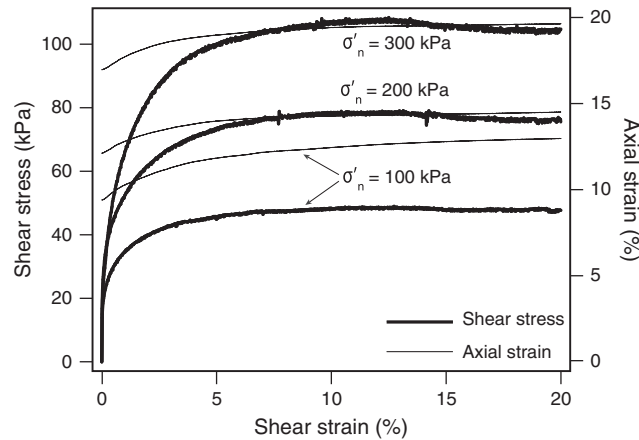


Figure 2. Stress-strain curves for monotonic, displacement-controlled direct shear tests at normal effective stresses (σ'_n) of 100, 200, and 300 kPa.

($\sigma'_n = 200$ kPa), and 108.41 kPa ($\sigma'_n = 300$ kPa). The Mohr Coulomb peak strength failure envelope is defined by an effective cohesion, c' , of 19.4 kPa and an effective friction angle, ϕ' , of 16.6° (Figure 3).

3.2. Dynamic Direct Shear Behavior

Following the consolidation stage ($\sigma'_n = 200$ kPa), each sample was monotonically sheared to 2% shear strain, broadly coincident with the onset of constant volume conditions. In the dynamic tests undertaken, this

normally consolidated hillslope sediments i.e., materials that have not experienced a greater effective compressive stress than that exerted by the existing overburden [Selby, 2005].

During consolidation, greater normal strains were observed with greater normal effective stresses (9.4% where $\sigma'_n = 100$ kPa; 12.1% where $\sigma'_n = 200$ kPa; 17.0% where $\sigma'_n = 300$ kPa). During the shearing stage, all samples continued to compress until peak shear strength was achieved, though the majority of normal strain occurred prior to achieving shear strains of 2–3%.

Observed peak strength values were 48.97 kPa ($\sigma'_n = 100$ kPa), 79.10 kPa

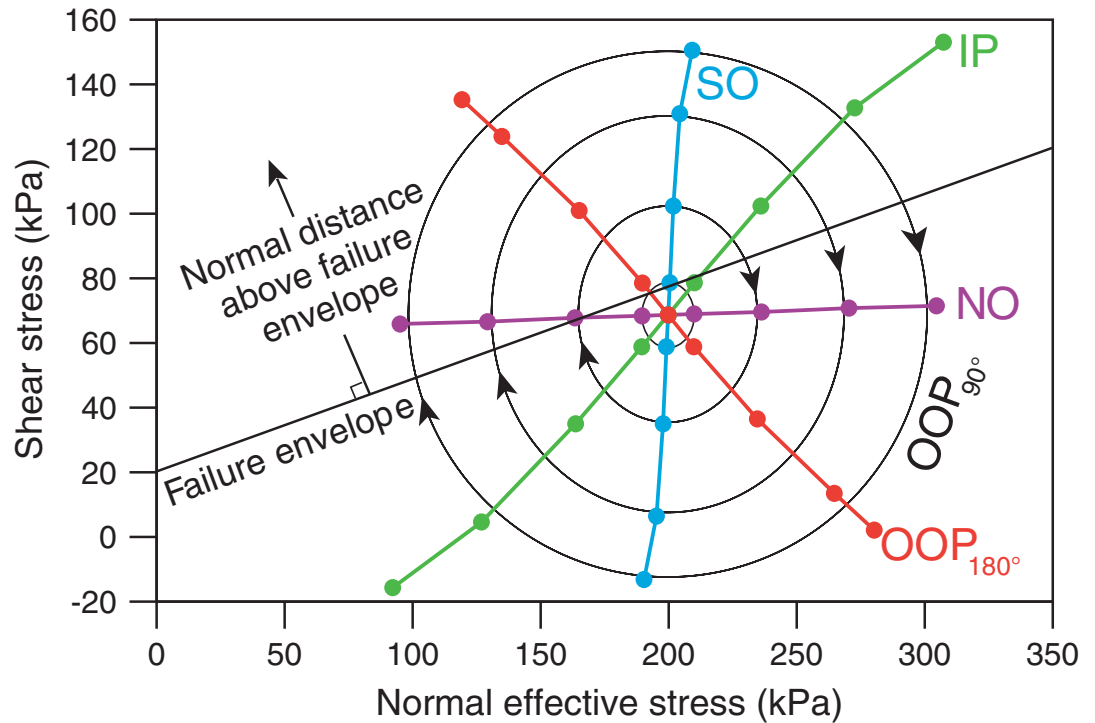


Figure 3. Idealized stress conditions in shear stress versus normal stress space during the dynamic stages of each of the tests undertaken, and relative to the monotonic Mohr-Coulomb failure envelope. Dynamic stress conditions are colored by wave-phasing scenario: normal-only (NO), shear-only (SO), in-phase (IP), 90° out-of-phase (OOP_{90°}), and 180° out-of-phase (OOP_{180°}) conditions (see text for further details). The initial stress state of each test lies at the intersection of the dynamic stress conditions. The stress amplitudes employed in each test are shown by the markers along each stress path for SO, IP, NO, and OOP_{180°} tests and by the radii of the concentric circles in the OOP_{180°} tests.

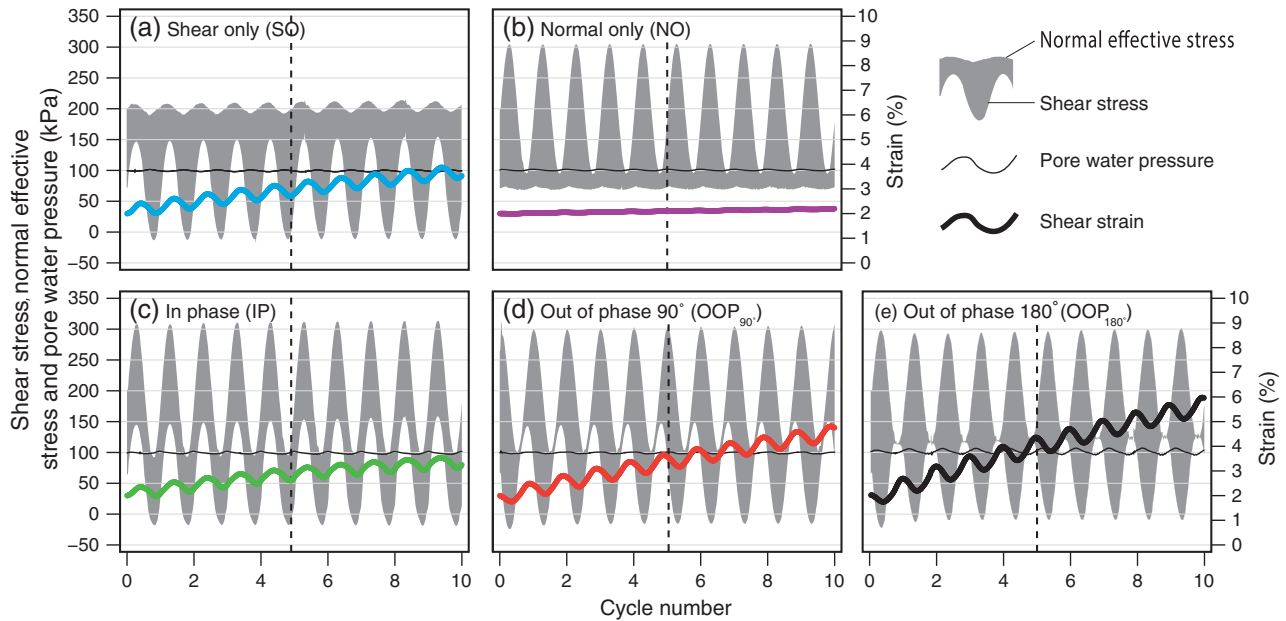


Figure 4. Variations in the stress state (shear stress and normal effective stress), pore water pressure, and shear strain as function of cycle number for the five dynamic tests undertaken using specified stress amplitudes of 105 kPa. The vertical dashed lines on each graph are provided to allow visual assessment of the phase offset between shear and normal effective stresses.

corresponded to an initial (baseline) shear stress of approximately 65–70 kPa, approximately 80–90% of the peak shear strength at this normal effective stress level (200 kPa). For the maximum baseline shear stress values observed, equivalent specified dynamic normal and shear stress amplitudes for each wave-phasing scenario were 10, 35, 70, and 105 kPa. Idealized stress conditions during the dynamic tests in shear stress versus normal stress space and relative to the Mohr-Coulomb failure envelope are displayed in Figure 3.

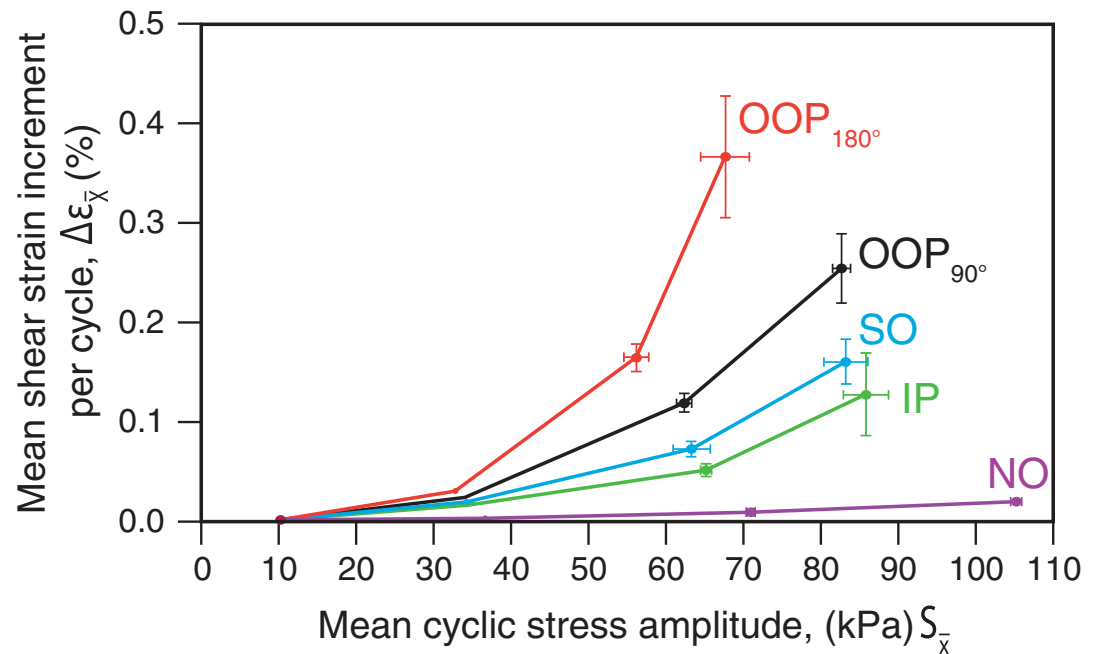


Figure 5. Variations in mean shear strain increment per cycle with mean cyclic stress amplitude for the full set of tests completed. For SO, IP, OOP_{90°}, and OOP_{180°}, cyclic stress amplitudes refer to shear stress only. For NO tests, mean cyclic stress amplitudes refer to normal stress only. Error bars indicate the standard deviation of the mean value for each data point.

We present variations in the stress state of the sample (shear stress and normal effective stress), pore water pressure and shear strain as a function of cycle number for the 105 kPa stress amplitude tests in Figure 4. The specified cyclic stress amplitudes are generally well controlled by the DynBPS, though we note that there are some minor responses in normal effective stress during the SO scenario. However, the amplitude (approximately 10 kPa) is small compared to the dynamic shear stresses applied and as such we do not consider this to be significant. We also note that shear stress amplitudes did not reach their specified targets in all tests (compare in particular shear stress amplitudes in Figures 4a and 4e). As we note below, this does not affect our conclusions.

We observed only minor (generally < 3 kPa; Figure 4) changes in pore pressure during each dynamic phase, indicating full transfer of variations in total to effective normal stress. The differences in response to the various wave phase relationships are pronounced. The lowest magnitude of shear strain accumulation is evident in the normal-only (NO) scenario (Figure 4b); the maximum is evident in the 180° out-of-phase (OOP $_{180^\circ}$) scenario (Figure 4e).

To further compare wave-phasing scenarios, we consider the mean shear strain increment per stress cycle ($\Delta\epsilon_{\bar{x}}$, %) as a function of the mean cyclic stress amplitude ($S_{\bar{x}}$, kPa) during the first 10 cycles of each test (Figure 5), prior to the onset of strain hardening or softening effects that are not considered here [Goodman and Seed, 1966]. We observe experimental variability in both $S_{\bar{x}}$ and $\Delta\epsilon_{\bar{x}}$, which we depict in Figure 5 using the standard deviation of the mean for each variable. Two key behaviors are evident. First, the magnitude of $\Delta\epsilon_{\bar{x}}$ increases nonlinearly with $S_{\bar{x}}$. Second, values of $\Delta\epsilon_{\bar{x}}$ diverge with increased values of $S_{\bar{x}}$ between the wave-phasing scenarios tested, most strongly when $S_{\bar{x}} > 35$ kPa. In all scenarios, small values of $\Delta\epsilon_{\bar{x}}$ ($< 0.003\%$) were observed where $S_{\bar{x}} \approx 10$ kPa.

In our benchmark data set SO (i.e., where we applied dynamic shear stress under constant normal stress conditions), the strain increment ($\Delta\epsilon_{\bar{x}}$) increases in a nonlinear manner with $S_{\bar{x}}$. The dynamic in-phase (IP) tests show a similar response to SO, but with reduced $\Delta\epsilon_{\bar{x}}$. This lower $\Delta\epsilon_{\bar{x}}$ response to $S_{\bar{x}}$ results from a synchronous increase in normal and shear stresses, where frictional resistance rises in phase with shear stress. The tests with a dynamic normal stress but static shear stress (NO) displays the smallest $\Delta\epsilon_{\bar{x}}$ response and the least pronounced nonlinearity of $\Delta\epsilon_{\bar{x}}$ with $S_{\bar{x}}$. The out-of-phase (OOP $_{90^\circ}$ and OOP $_{180^\circ}$) experimental series show considerable differences in $\Delta\epsilon_{\bar{x}}$. In both cases $\Delta\epsilon_{\bar{x}}$ is substantially larger than for SO and a greater degree of nonlinearity with increased $S_{\bar{x}}$ is observed. In OOP $_{180^\circ}$, peak shear stress is coincident with the minimum frictional resistance to shear, such that it develops very large values of $\Delta\epsilon_{\bar{x}}$ compared with the other scenarios. In OOP $_{90^\circ}$ shear stress and normal stress are 90° out of phase, such that shear stress peaks when normal stress is at its baseline value, and vice versa. Such conditions favor the development of greater values of $\Delta\epsilon_{\bar{x}}$ than SO, yet not as great as OOP $_{180^\circ}$.

The high magnitude of $\Delta\epsilon_{\bar{x}}$ during OOP $_{180^\circ}$ experiments prevented the specified $S_{\bar{x}}$ targets of 35 kPa, 70 kPa, and 105 kPa from being achieved, but this does not invalidate the results. Indeed, maximum $S_{\bar{x}}$ in OOP $_{180^\circ}$ was 68 kPa, yet the resultant $\Delta\epsilon_{\bar{x}}$ remains the highest observed ($0.36\% \pm 0.06$), even when compared to other scenarios that achieved greater $S_{\bar{x}}$. Extrapolating the tendency in $\Delta\epsilon_{\bar{x}}$ with $S_{\bar{x}}$ for OOP $_{180^\circ}$ suggests values of $\Delta\epsilon_{\bar{x}}$ that are at least an order of magnitude greater than those observed in OOP $_{90^\circ}$, SO, and IP for $S_{\bar{x}}$ of approximately 85 kPa. Specified normal stress amplitudes were consistently reached (Figure 4) during NO due to lower total normal strain accumulation ($\pm 0.5\%$ from initial values).

4. Instantaneous Stress State and Nonlinear Strain Rate

The observed differences in $\Delta\epsilon_{\bar{x}}$ can be partly explained with reference to the dynamic stress state of each wave-phasing scenario relative to the monotonic failure envelope (Figure 3). Where $S_{\bar{x}} = 10$ kPa, none of the tests underwent observable shear strain, suggesting that measureable shear strain only accumulates when the dynamic stress path crosses the failure envelope into unstable stress states. This principle is further demonstrated by the NO tests, which only clearly accumulated measurable strain where $S_{\bar{x}} > 35$ kPa and the dynamic stress path crossed the failure envelope. In all other tests, clear shear strain was observed, but considerable variations in $\Delta\epsilon_{\bar{x}}$ were noted. These differences are associated with the distance normal to the failure envelope that the stress condition of each test achieved; the greater the distance, the greater the value of $\Delta\epsilon_{\bar{x}}$.

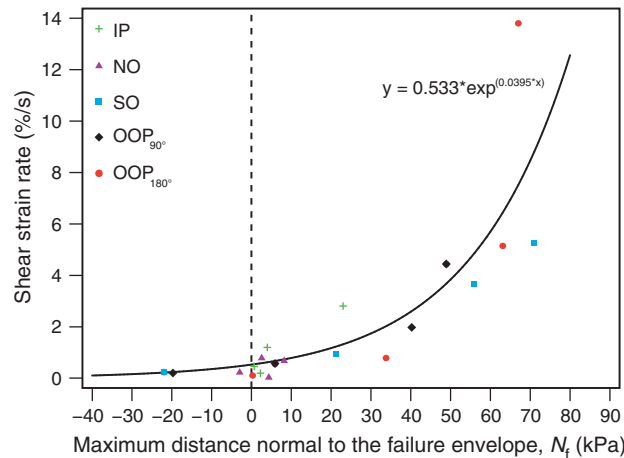


Figure 6. Maximum shear strain rate observed in each of the 20 dynamic tests plotted against maximum distance normal to the Mohr-Coulomb failure envelope (N_f). The vertical dashed line indicates the position of the failure envelope. Positive values of N_f indicate unstable stress states located above the failure envelope. Negative values of N_f indicate stable stress states located below the failure envelope.

We investigated this phenomenon further by considering how instantaneous strain rate (%/s) varies with distance normal to the failure envelope, N_f (kPa). We calculated N_f as

$$N_f = \frac{\tau_1 - m\sigma'_{n1} - c'}{\sqrt{m^2 + 1}} \quad (3)$$

where τ_1 is the instantaneous value of shear stress (in kPa), σ'_{n1} is the instantaneous value of normal effective stress (in kPa), m is the tangent of the friction angle (expressed in radians), and c' is the effective cohesion (in kPa). Positive values of N_f indicate “unstable” stress states located “above” the failure envelope in plots of shear stress against normal effective stress. In contrast, negative values of N_f indicate “stable” stress states located “below” the failure envelope.

For each of the 20 dynamic tests undertaken, we determined the maximum observed shear strain rate and subsequently calculated the corresponding value of N_f . From Figure 6, it is evident that shear strain rate is a nonlinear (exponential) function of N_f . Combinations of shear stress and normal effective stress that yield negative or low positive (<10 kPa) values of N_f such that the stress state is stable or marginally unstable, generate low shear strain rates. This explains the low values of $\Delta\epsilon_{\bar{x}}$ where $S_{\bar{x}}$ is low and/or where the wave-phasing characteristics cause N_f to remain low. However, greater positive values of N_f result in an exponential increase in strain rate and strain accumulation. This explains the observed nonlinearity in $\Delta\epsilon_{\bar{x}}$ with increasing $S_{\bar{x}}$; a small increase in N_f causes a disproportionate increase in strain rate and, hence, $\Delta\epsilon_{\bar{x}}$, particularly in the OOP_{180°} tests.

The strong ($r^2_{adj} = 0.67$) and statistically significant ($p < 0.0001$) exponential relationship between shear strain rate and N_f (Figure 6) is based on results from all wave-phasing scenarios tested, suggesting that the relationship observed is universal and independent of instantaneous wave phasing. However, the greatest shear strain rate observed (13.8%/s; OOP_{180°}) is more than twice that of other tests that achieved a similar value of N_f . It is important to determine whether this has resulted from experimental variability and/or our treatment of the data to only consider the maximum observed strain rate values in each dynamic test, or whether this results from systematic differences in shear strain rate that depend on wave-phasing relationships. In Figure 7, we have expanded our analysis to consider the relationship between shear strain rate and N_f throughout the dynamic stage of each test. For clarity in presentation, we applied a 0.05 s running mean to both N_f and shear strain rate data; this results in reduced peak values but here we are interested in the form of the plots, having considered maxima in Figure 6. In Figures 7a (10 kPa stress amplitude) and 7b (35 kPa stress amplitude), we observed little difference in the range of strain rates observed between wave-phasing scenarios, which corresponds to the minor differences in $\Delta\epsilon_{\bar{x}}$ observed at the equivalent stress amplitudes (10 kPa and 35 kPa) in Figure 5. In Figures 7c (70 kPa stress amplitude) and 7d (105 kPa stress amplitude), differences in the form of the plots for different wave-phasing scenarios are more evident. The shear strain rate is not solely a function of N_f . It also depends on the instantaneous wave-phasing scenario. For the OOP_{180°} tests in particular, higher values of shear strain rate are achieved for a given value of N_f than in the SO and OOP_{90°} tests. Furthermore, for the OOP_{180°} tests, the strain rate continues to increase nonlinearly until the maximum value of N_f is achieved. This contrasts with the SO and OOP_{90°} test results; strain rates are lower and peak and decrease before the maximum value of N_f is achieved.

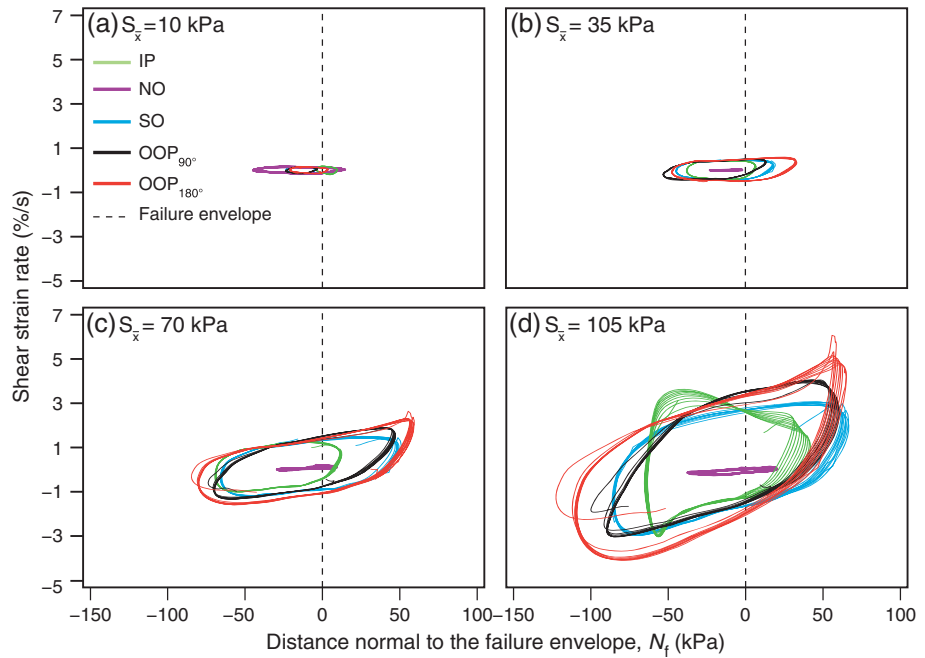


Figure 7. (a–d) Shear strain rate throughout the dynamic stage of each test plotted against distance normal to the Mohr-Coulomb failure envelope (N_f) for cyclic stress amplitudes (S_x) of different magnitude. The vertical dashed line indicates the position of the failure envelope. Positive values of N_f indicate unstable stress states located above the failure envelope. Negative values of N_f indicate stable stress states located below the failure envelope. Prior to plotting, and for clarity, a 0.05 s running mean was applied to both shear strain rate and N_f variables.

5. Discussion

Using the DynBPS apparatus to simulate a range of wave-phasing scenarios, our results demonstrate that the phase relationship between dynamic effective normal and shear stresses has a significant control on coseismic strain accumulation in landslides. Variably phased effective normal and shear stresses control the instantaneous stress state within a sample. In turn, this affects both the instantaneous strain rate and the trajectory of the strain rate which, when integrated with respect to time, can produce considerable differences in accumulated shear strain (Figure 5). Critically, we have demonstrated that the effects of wave phasing on coseismic shear strain scale nonlinearly with loading magnitude, such that the increased shear strain effects are most pronounced when dynamic normal and shear stress amplitudes at the rupture surface are simultaneously at their maxima and out of phase. In other words, instantaneously out-of-phase high-magnitude dynamic normal effective and shear stresses cause a disproportionately large landslide strain accumulation response. We attribute these effects to a strong positive feedback mechanism by which a reduction in the formation of strong frictional contacts [Hencher, 1977, cited in Hencher, 2012] and/or normal force chain networks [Estep and Dufek, 2012] occurs in response to a decrease in normal effective stress. This causes the observed increase in shear strain rate which, in turn, further reduces the ability of frictional contacts to establish [Hencher, 1977, cited in Hencher, 2012].

A key implication of the nonlinearity observed in our results is that a single loading cycle of high-magnitude, out-of-phase normal effective and shear stresses is not canceled out by a single, equal-magnitude loading cycle in which normal effective and shear stresses are in phase. The implicit assumption in recent applications of the *Newmark* [1965] sliding block model that the effects of slope-normal accelerations can be ignored through time as the resultant enhanced (out of phase) or reduced (in phase) displacements cancel out over the duration of an earthquake [see Jibson, 2011; Matasovic et al., 1998] is incorrect. This is because coseismic strain accumulation (and, by implication, D_N) during out-of-phase dynamic normal effective and shear stresses can be exponentially greater than that resulting from comparable magnitude in-phase dynamic normal effective and shear stresses.

Conventional *Newmark* [1965] analysis that considers slope-parallel accelerations (and hence shear stresses) only represents a specific case of coseismic hillslope loading conditions because of the results of variable normal effective and shear stress wave phasing. Use of the conventional *Newmark* [1965] model may therefore generate considerable inaccuracies when determining D_N . In circumstances where dynamic normal effective and shear stresses are out-of-phase, conventional *Newmark* [1965] analysis is likely to underpredict D_N . Conversely, our results demonstrate that D_N may be conventionally overpredicted where equal-amplitude normal and shear stresses are predominantly in phase.

We note that the effect of the instantaneous normal effective and shear stress wave-phasing relationship is not the only potential source of error in estimations of coseismic landslide displacement. Differences between observed and predicted landslide occurrence can also result from seismogenic characteristics, such as fault type and depth [Keefer, 1984]; regional contrasts in seismic wave attenuation, lithology/shear strength, and antecedent conditions [Schulz and Wang, 2014; Dreyfus et al., 2013; Malamud et al., 2004; Meunier et al., 2007]; and local site effects, such as topographic amplification [Buech et al., 2010; Harp and Jibson, 2002; McColl et al., 2012; Meunier et al., 2008; Sepúlveda et al., 2005a, 2005b], internal landslide mass amplification effects [Bray and Travararou, 2007; Rathje and Bray, 2000] and undrained dynamic shear behavior during ground shaking (i.e., elevated pore water pressure effects) [Trandafir and Sassa, 2005; Danneels et al., 2008; Wang and Sassa, 2009]. These processes and effects are also widely regarded to be significant controls on the scatter observed in regional-scale correlations between landsliding and earthquake magnitude and/or Peak Ground Acceleration [Keefer, 1984; Meunier et al., 2007; Rodríguez et al., 1999]. Wave-phasing effects are part of this suite of controls on coseismic landslide occurrence, though its relative efficacy in driving coseismic strain accumulation is currently poorly understood, and likely to be highly variable, at both local to regional scales. However, the diversity (potentially up to an order of magnitude) in coseismic strain accumulation resulting from wave-phasing effects demonstrated here may be comparable to, or even be sufficient to overprint, other controls on the location and nature of coseismic landsliding. This suggests that the wave-phasing phenomenon investigated here requires further research at both hillslope and orogen scales.

Since the observed differences in strain accumulation are a function of normal effective stress, we note that the wave-phasing effect we report is applicable to only the frictional component of shear strength. As such, our findings are primarily applicable to lithologies and slope settings where the shear strength results primarily from friction [see Milledge et al., 2014]. In addition, our findings are most applicable to drained or unsaturated shear surfaces rather than situations where pore pressure rapidly elevates during coseismic ground shaking (i.e., when undrained conditions occur) and causes normal effective stress to reduce significantly [Trandafir and Sassa, 2005; Danneels et al., 2008; Wang and Sassa, 2009].

The mechanisms and conditions that may promote local to regional differences in normal and shear stress wave phasing may include, for example, polarization, attenuation and amplification of seismic waves [Bokelmann and Harjes, 2000; Burjánek et al., 2012; Jibson and Harp, 2012; McColl et al., 2012; Moore et al., 2011], or the interaction and modification (diffraction and/or interference) of incident seismic waves with topography [Bourdeau and Havenith, 2008; Del Gaudio and Wasowski, 2011; Lenti and Martino, 2012, 2013; Meunier et al., 2008; Xu et al., 2011]. Information describing how slope-normal and slope-parallel wave phasing is distributed across the landscape and how this correlates with the spatial distribution of coseismic landslide displacements can provide improvements to understanding the regional-scale impacts of earthquakes on slopes [cf. Jibson, 2007]. At present, however, the probability of occurrence during earthquake shaking and spatial distribution of variably phased cyclic slope-normal and slope-parallel stresses are poorly understood. Obtaining such information is critical because the wave-phasing effect is dependent on the instantaneous wave phase offset between normal effective and shear stresses. As such, proxies for coseismic ground accelerations, such as Arias [1970] intensity, are insufficient to permit assessment of instantaneous wave-phasing relationships. However, such information can be obtained with a dense regional network of seismometers located on hillslopes likely to be affected by earthquake ground accelerations. Moore et al. [2011] and Burjánek et al. [2012], for example, have undertaken analysis of seismic records obtained from installations on rockslide at Randa, Switzerland. Data obtained from a regional network of such installations on slopes of varying character, such as lithology, slope angle, distance, and aspect relative to the earthquake epicenter, will permit the regional spatial pattern of

wave-phasing to be determined. Such studies are a critical first step in assessing the landform- and landscape-scale significance of the normal and shear stress wave-phasing effect on the magnitude of coseismic landslide displacement. Subsequently, and when used in conjunction with laboratory and modeling studies that describe how seismic waves interact with topography and shear surfaces [Hildyard and Young, 2002; Meunier et al., 2008; Nakagawa et al., 2000], the effects of wave phasing can be fed into regional assessments of coseismic landslide hazard [Dreyfus et al., 2013; Jibson et al., 2000] to improve predictive capacity.

6. Conclusions

In this paper, we have assessed the significance of the instantaneous phase offset between coseismic (dynamic) slope-normal and slope-parallel stresses on the magnitude of coseismic landslide displacement. We used a bespoke geotechnical testing apparatus (the Dynamic Back-Pressured Shearbox; DynBPS) to subject sediment samples to variably phased normal and shear stresses under direct shear conditions. Our key findings and conclusions are as follows:

1. The instantaneous phase relationship between dynamic effective normal and shear stresses is a key control on the magnitude of coseismic strain accumulation in landslides. Greater strain results when effective normal and shear stresses are simultaneously at their maxima and fully out of phase. In contrast, in-phase effective normal and shear dynamic stresses reduce observed shear strain relative to same-amplitude loading cycles during which shear stress is varied but effective normal stress remains constant.
2. Out-of-phase, high-magnitude dynamic normal effective and shear stresses cause a disproportionately large-strain response, relative to shear-only conditions or those in which normal effective and shear stresses are in phase. This can be explained by nonlinear strain rates. We have demonstrated that strain rate is an exponential function of the distance normal to the (monotonic shear) Mohr-Coulomb failure envelope in plots of shear stress against normal effective stress. Critically, this distance is strongly controlled by the phase offset between dynamic normal and shear stresses. We suggest a positive feedback mechanism by which a reduced normal effective stress limits the formation of strong frictional contacts between sediment grains. This allows the shear strain rate to increase, which further reduces the ability of frictional contacts to establish. Since the wave-phasing effect we observe controls frictional strength, our results are most likely to be applicable in Earth materials and slope settings in which frictional strength dominates relative to the cohesive component of shear strength, and where drained conditions are prevalent.
3. The observed nonlinearity in strain rate has important implications for existing models of coseismic landslide displacement, such as that developed by *Newmark* [1965]. We have shown that a single loading cycle of high-magnitude, out-of-phase normal effective and shear stresses is not balanced by a single, equal-magnitude loading cycle characterized by in-phase normal effective and shear stresses. The implicit assumption of conventional *Newmark* [1965] that analysis can use slope-parallel (shear-only) ground accelerations only is not valid; the strain accumulated by a fully out-of-phase wave cycle is not canceled out by a cycle in which wave amplitudes are the same, but in phase.
4. Conventional coseismic slope stability models that ignore the influence of normal and shear stress wave phasing (such as *Newmark* [1965]) may either significantly overestimate or underestimate earthquake-induced landslide displacement, by up to an order of magnitude. This has important implications for accurate assessment of coseismic landslide hazard.
5. In order to improve local to regional assessments of the susceptibility of landslide to deformation during earthquakes, future work should focus on the deployment and analysis of a regional network of seismometers located on hillslopes to determine whether predictable spatial patterns in wave phasing occur at the landform and landscape scales.

Acknowledgments

Petley was funded by the NERC Earthquakes Without Frontiers project, grant NE/J01995Z/1. Data used in this paper can be obtained by request from the corresponding author. We are grateful to Alex Densmore for his helpful feedback on an earlier draft of the manuscript, and to Simon Brain for mathematical advice. We also thank two anonymous reviewers for their constructive comments.

References

- Ambraseys, N. N., and J. M. Menu (1988), Earthquake-induced ground displacements, *Earthquake Eng. Struct. Dyn.*, *16*(7), 985–1006, doi:10.1002/eqe.4290160704.
- Aoi, S., T. Kunugi, and H. Fujiwara (2008), Trampoline effect in extreme ground motion, *Science*, *322*(5902), 727–730.
- Arias, A. (1970), Measure of earthquake intensity, in *Seismic Design for Nuclear Power Plants*, edited by R. J. Hansen, pp. 438–483, Massachusetts Institute of Technology Press, Cambridge, Mass.

- Barla, G., M. Barla, and M. E. Martinotti (2010), Development of a new direct shear testing apparatus, *Rock Mech. Rock Eng.*, *43*, 117–122, doi:10.1007/s00603-009-0041-5.
- Blott, S. J., and K. Pye (2001), GRADISTAT: A grain size distribution and statistics package for the analysis of unconsolidated sediments, *Earth Surf. Processes Landforms*, *26*(11), 1237–1248, doi:10.1002/esp.261.
- Bokelmann, G. H. R., and H.-P. Harjes (2000), Evidence for temporal variation of seismic velocity within the upper continental crust, *J. Geophys. Res.*, *105*(B10), 23,879–23,894, doi:10.1029/2000JB900207.
- Bourdeau, C., and H. B. Havenith (2008), Site effects modelling applied to the slope affected by the Suusamyr earthquake (Kyrgyzstan, 1992), *Eng. Geol.*, *97*(3–4), 126–145, doi:10.1016/j.enggeo.2007.12.009.
- Bradley, B. A., and M. Cubrinovski (2011), Near-source strong ground motions observed in the 22 February 2011 Christchurch earthquake, *Seismol. Res. Lett.*, *82*(6), 853–865, doi:10.1785/gssrl.82.6.853.
- Bray, J., and T. Travararou (2007), Simplified procedure for estimating earthquake-induced deviatoric slope displacements, *J. Geotech. Geoenviron. Eng.*, *133*(4), 381–392, doi:10.1061/(ASCE)1090-0241(2007)133:4(381).
- British Standards Institution (1999), *BS 5930: Code of Practice for Site Investigations*, British Standards Institution, London.
- Buech, F., T. R. Davies, and J. R. Pettinga (2010), The Little Red Hill seismic experimental study: Topographic effects on ground motion at a bedrock-dominated mountain edifice, *Bull. Seismol. Soc. Am.*, *100*(5A), 2219–2229, doi:10.1785/0120090345.
- Burjānek, J., J. R. Moore, F. X. Yugsi Molina, and D. Fäh (2012), Instrumental evidence of normal mode rock slope vibration, *Geophys. J. Int.*, *188*(2), 559–569, doi:10.1111/j.1365-246X.2011.05272.x.
- Burland, J. B. (1990), On the compressibility and shear strength of natural clays, *Geotechnique*, *40*(3), 329–378.
- Christakos, G. (2003), Soil behaviour under dynamic loading conditions: Experimental procedures and statistical trends, *Stochastic Environ. Res. Risk Assess.*, *17*(3), 175–190, doi:10.1007/s00477-003-0132-x.
- Danneels, G., C. Bourdeau, I. Torgoev, and H.-B. Havenith (2008), Geophysical investigation and dynamic modelling of unstable slopes: Case-study of Kainama (Kyrgyzstan), *Geophys. J. Int.*, *175*(1), 17–34, doi:10.1111/j.1365-246X.2008.03873.x.
- Del Gaudio, V., and J. Wasowski (2011), Advances and problems in understanding the seismic response of potentially unstable slopes, *Eng. Geol.*, *122*(1–2), 73–83, doi:10.1016/j.enggeo.2010.09.007.
- Dreyfus, D., E. M. Rathje, and R. W. Jibson (2013), The influence of different simplified sliding-block models and input parameters on regional predictions of seismic landslides triggered by the Northridge earthquake, *Eng. Geol.*, *163*, 41–54, doi:10.1016/j.enggeo.2013.05.015.
- Estep, J., and J. Dufek (2012), Substrate effects from force chain dynamics in dense granular flows, *J. Geophys. Res.*, *117*, F01028, doi:10.1029/2011JF002125.
- Friedman, G. M., and F. E. Sanders (1978), *Principles of Sedimentology*, 792 pp., Wiley, New York.
- Gan, J. K. M., D. G. Fredlund, and D. G. Rahardjo (1988), Determination of the shear strength parameters of an unsaturated soil using the direct shear test, *Can. Geotech. J.*, *25*, 500–510.
- Goodman, R. E., and H. B. Seed (1966), Earthquake-induced displacements in sand embankments, *J. Soil Mech. Found. Div.*, *92*(SM2), 125–146.
- Guzzetti, F., A. Carrara, M. Cardinali, and P. Reichenbach (1999), Landslide hazard evaluation: A review of current techniques and their application in a multi-scale study, Central Italy, *Geomorphology*, *31*(1–4), 181–216, doi:10.1016/S0169-555X(99)00078-1.
- Harp, E. L., and R. W. Jibson (2002), Anomalous concentrations of seismically triggered rock falls in Pacoima Canyon: Are they caused by highly susceptible slopes or local amplification of seismic shaking?, *Bull. Seismol. Soc. Am.*, *92*(8), 3180–3189.
- Head, K. H., and R. Epps (2011), *Manual of Soil Laboratory Testing Volume Two: Permeability, Shear Strength and Compressibility Tests*, 480 pp., Taylor and Francis, London.
- Hencher, S. (1977), The effect of vibration on the friction between rock surfaces, Unpublished PhD thesis, Imperial College of Science and Technology, London Univ.
- Hencher, S. (2012), *Practical Engineering Geology*, Spon Press/Taylor and Francis, London and New York.
- Hildyard, M., and R. P. Young (2002), Modelling seismic waves around underground openings in fractured rock, in *The Mechanism of Induced Seismicity*, edited by C. Trifu, pp. 247–276, Birkhäuser, Basel, doi:10.1007/978-3-0348-8179-1_12.
- Hovius, N., P. Meunier, C.-W. Lin, H. Chen, Y.-G. Chen, S. Dadson, M.-J. Horng, and M. Lines (2011), Prolonged seismically induced erosion and the mass balance of a large earthquake, *Earth Planet. Sci. Lett.*, *304*(3–4), 347–355, doi:10.1016/j.epsl.2011.02.005.
- Huang, C. C., Y. H. Lee, H. P. Liu, D. K. Keefer, and R. W. Jibson (2001), Influence of surface-normal ground acceleration on the initiation of the Jih-Feng-Erh-Shan landslide during the 1999 Chi-Chi, Taiwan, earthquake, *Bull. Seismol. Soc. Am.*, *91*(5), 953–958, doi:10.1785/0120000719.
- Hyde, A., T. Higuchi, and K. Yasuhara (2006), Liquefaction, cyclic mobility, and failure of silt, *J. Geotech. Geoenviron. Eng.*, *132*(6), 716–735, doi:10.1061/(ASCE)1090-0241(2006)132:6(716).
- Ingles, J., J. Darrozes, and J.-C. Soula (2006), Effects of the vertical component of ground shaking on earthquake-induced landslide displacements using generalized Newmark analysis, *Eng. Geol.*, *86*(2–3), 134–147, doi:10.1016/j.enggeo.2006.02.018.
- Jibson, R. W. (1993), Predicting earthquake-induced landslide displacements using Newmark's sliding block analysis, *Transp. Res. Rec.*, *1411*, 9–17.
- Jibson, R. W. (2007), Regression models for estimating coseismic landslide displacement, *Eng. Geol.*, *91*(2–4), 209–218, doi:10.1016/j.enggeo.2007.01.013.
- Jibson, R. W. (2011), Methods for assessing the stability of slopes during earthquakes—A retrospective, *Eng. Geol.*, *122*(1–2), 43–50, doi:10.1016/j.enggeo.2010.09.017.
- Jibson, R. W., and E. L. Harp (2012), Extraordinary distance limits of landslides triggered by the 2011 mineral, Virginia, Earthquake, *Bull. Seismol. Soc. Am.*, *102*(6), 2368–2377, doi:10.1785/0120120055.
- Jibson, R. W., E. L. Harp, and J. A. Michael (2000), A method for producing digital probabilistic seismic landslide hazard maps, *Eng. Geol.*, *58*(3–4), 271–289, doi:10.1016/S0013-7952(00)00039-9.
- Keefer, D. K. (1984), Landslides caused by earthquakes, *Geol. Soc. Am. Bull.*, *95*(4), 406–421, doi:10.1130/0016-7606(1984)95<406:lcb>2.0.co;2.
- Keefer, D. K. (1994), The importance of earthquake-induced landslides to long-term slope erosion and slope-failure hazards in seismically active regions, *Geomorphology*, *10*(1–4), 265–284, doi:10.1016/0169-555X(94)90021-3.
- Lenti, L., and S. Martino (2012), The interaction of seismic waves with step-like slopes and its influence on landslide movements, *Eng. Geol.*, *126*, 19–36, doi:10.1016/j.enggeo.2011.12.002.
- Lenti, L., and S. Martino (2013), A parametric numerical study of the interaction between seismic waves and landslides for the evaluation of the susceptibility to seismically induced displacements, *Bull. Seismol. Soc. Am.*, *103*(1), 33–56, doi:10.1785/0120120019.
- Li, G., A. J. West, A. L. Densmore, Z. Jin, R. N. Parker, and R. G. Hilton (2014), Seismic mountain building: Landslides associated with the 2008 Wenchuan earthquake in the context of a generalized model for earthquake volume balance, *Geochem. Geophys. Geosyst.*, *15*, 833–844, doi:10.1002/2013GC005067.

- Liao, C.-J., D.-H. Lee, J.-H. Wu, and C.-Z. Lai (2011), A new ring-shear device for testing rocks under high normal stress and dynamic conditions, *Eng. Geol.*, *122*(1–2), 93–105, doi:10.1016/j.enggeo.2011.03.018.
- Malamud, B. D., D. L. Turcotte, F. Guzzetti, and P. Reichenbach (2004), Landslides, earthquakes, and erosion, *Earth Planet. Sci. Lett.*, *229*(1–2), 45–59, doi:10.1016/j.epsl.2004.10.018.
- Marano, K., D. Wald, and T. Allen (2010), Global earthquake casualties due to secondary effects: A quantitative analysis for improving rapid loss analyses, *Nat. Hazards*, *52*(2), 319–328, doi:10.1007/s11069-009-9372-5.
- Matasovic, N., E. Kavazanjian, and J. P. Giroud (1998), Newmark seismic deformation analysis for geosynthetic covers, *Geosynth. Int.*, *5*(1–2), 237–264.
- McColl, S. T., T. R. H. Davies, and M. J. McSaveney (2012), The effect of glaciation on the intensity of seismic ground motion, *Earth Surf. Processes Landforms*, *37*(12), 1290–1301, doi:10.1002/esp.3251.
- Meunier, P., N. Hovius, and A. J. Haines (2007), Regional patterns of earthquake-triggered landslides and their relation to ground motion, *Geophys. Res. Lett.*, *34*, L20408, doi:10.1029/2007GL031337.
- Meunier, P., N. Hovius, and J. A. Haines (2008), Topographic site effects and the location of earthquake induced landslides, *Earth Planet. Sci. Lett.*, *275*(3–4), 221–232, doi:10.1016/j.epsl.2008.07.020.
- Milledge, D. G., D. Bellugi, J. A. McKean, A. L. Densmore, and W. E. Dietrich (2014), A multidimensional stability model for predicting shallow landslide size and shape across landscapes, *J. Geophys. Res. Earth Surf.*, *119*, 2481–2504, doi:10.1002/2014JF003135.
- Moore, J. R., V. Gischig, J. Burjanek, S. Loew, and D. Fäh (2011), Site effects in unstable rock slopes: Dynamic behavior of the Randa instability (Switzerland), *Bull. Seismol. Soc. Am.*, *101*(6), 3110–3116, doi:10.1785/0120110127.
- Nakagawa, S., K. T. Nihei, and L. R. Myer (2000), Shear-induced conversion of seismic waves across single fractures, *Int. J. Rock Mech. Min. Sci.*, *37*(1–2), 203–218, doi:10.1016/S1365-1609(99)00101-X.
- Newmark, N. M. (1965), Effects of earthquakes on dams and embankments, *Geotechnique*, *15*(2), 139–160.
- Parker, R. N., A. L. Densmore, N. J. Rosser, M. de Michele, Y. Li, R. Huang, S. Whadcoat, and D. N. Petley (2011), Mass wasting triggered by the 2008 Wenchuan earthquake is greater than orogenic growth, *Nat. Geosci.*, *4*(7), 449–452, doi:10.1038/ngeo1154.
- Petley, D. N. (2012), Global patterns of loss of life from landslides, *Geology*, doi:10.1130/g33217.1.
- Powrie, W. (2004), *Soil Mechanics: Concepts and Applications*, 440 pp., Spon Press/Taylor and Francis Group, London and New York.
- Rathje, E., and J. Bray (2000), Nonlinear coupled seismic sliding analysis of Earth structures, *J. Geotech. Geoenviron. Eng.*, *126*(11), 1002–1014, doi:10.1061/(ASCE)1090-0241(2000)126:11(1002).
- Rathje, E. M., and G. Antonakos (2011), A unified model for predicting earthquake-induced sliding displacements of rigid and flexible slopes, *Eng. Geol.*, *122*(1–2), 51–60, doi:10.1016/j.enggeo.2010.12.004.
- Rathje, E. M., and G. Saygili (2009), Probabilistic assessment of earthquake-induced sliding displacements of natural slopes, *Bull. New Zealand Soc. Earthquake Eng.*, *41*, 18–27.
- Rodriguez, C. E., J. J. Bommer, and R. J. Chandler (1999), Earthquake-induced landslides: 1980–1997, *Soil Dyn. Earthquake Eng.*, *18*(5), 325–346, doi:10.1016/S0267-7261(99)00012-3.
- Romeo, R. (2000), Seismically induced landslide displacements: A predictive model, *Eng. Geol.*, *58*(3–4), 337–351, doi:10.1016/S0013-7952(00)00042-9.
- Sağlam, S., and B. S. Bakır (2014), Cyclic response of saturated silts, *Soil Dyn. Earthquake Eng.*, *61*–62, 164–175, doi:10.1016/j.soildyn.2014.02.011.
- Sassa, K., H. Fukuoka, G. Wang, and N. Ishikawa (2004), Undrained dynamic-loading ring-shear apparatus and its application to landslide dynamics, *Landslides*, *1*(1), 7–19, doi:10.1007/s10346-003-0004-y.
- Saygili, G., and E. M. Rathje (2008), Empirical predictive models for earthquake-induced sliding displacements of slopes, *J. Geotech. Geoenviron. Eng.*, *134*, 790–803.
- Schulz, W. H., and G. Wang (2014), Residual shear strength variability as a primary control on movement of landslides reactivated by earthquake-induced ground motion: Implications for coastal Oregon, U.S., *J. Geophys. Res. Earth Surf.*, *119*, 1617–1635, doi:10.1002/2014JF003088.
- Selby, M. J. (2005), *Hillslope Materials and Processes*, Oxford Univ. Press, Oxford.
- Sepúlveda, S. A., W. Murphy, R. W. Jibson, and D. N. Petley (2005a), Seismically induced rock slope failures resulting from topographic amplification of strong ground motions: The case of Pacoima Canyon, California, *Eng. Geol.*, *80*(3–4), 336–348, doi:10.1016/j.enggeo.2005.07.004.
- Sepúlveda, S. A., W. Murphy, and D. N. Petley (2005b), Topographic controls on coseismic rock slides during the 1999 Chi-Chi earthquake, Taiwan, *Q. J. Eng. Geol. Hydrogeol.*, *38*(2), 189–196, doi:10.1144/1470-9236/04-062.
- Taylor, D. W. (1948), *Fundamentals of Soil Mechanics*, Wiley, New York.
- Trandafir, A. C., and K. Sassa (2005), Seismic triggering of catastrophic failures on shear surfaces in saturated cohesionless soils, *Can. Geotech. J.*, *42*, 229–251.
- Wang, G., and K. Sassa (2009), Seismic loading impacts on excess pore-water pressure maintain landslide triggered flowslides, *Earth Surf. Processes Landforms*, *34*(2), 232–241, doi:10.1002/esp.1708.
- Wartman, J., R. Seed, and J. Bray (2005), Shaking table modeling of seismically induced deformations in slopes, *J. Geotech. Geoenviron. Eng.*, *131*(5), 610–622, doi:10.1061/(ASCE)1090-0241(2005)131:5(610).
- Wasowski, J., D. K. Keefer, and C.-T. Lee (2011), Toward the next generation of research on earthquake-induced landslides: Current issues and future challenges, *Eng. Geol.*, *122*(1–2), 1–8, doi:10.1016/j.enggeo.2011.06.001.
- Wilson, R. C., and D. K. Keefer (1983), Dynamic analysis of a slope failure from the 6 August 1979 Coyote Lake, California, earthquake, *Bull. Seismol. Soc. Am.*, *73*(3), 863–877.
- Xu, Q., S. Zhang, and W. Li (2011), Spatial distribution of large-scale landslides induced by the 5.12 Wenchuan Earthquake, *J. Mt. Sci.*, *8*(2), 246–260, doi:10.1007/s11629-011-2105-8.
- Yuan, R.-m., C.-L. Tang, and Q.-h. Deng (2014), Effect of the acceleration component normal to the sliding surface on earthquake-induced landslide triggering, *Landslides*, *1*–10, doi:10.1007/s10346-014-0486-9.